International Journal of Neural Systems
♥World Scientific Publishing Company

CEREBROVASCULAR PATTERN IMPROVED BY OZONE AUTOHEMOTHERAPY: AN ENTROPY-BASED STUDY ON MULTIPLE SCLEROSIS PATIENTS

FILIPPO MOLINARI[*]
Corresponding Author, Biolab, Department of Electronics and Telecommunications, Politecnico di Torino, Corso Duca degli Abruzzi 24, 10129 Torino, Italy (Email: filippo.molinari@polito.it)

DANIELE RIMINI
Biolab, Department of Electronics and Telecommunications, Politecnico di Torino, Corso Duca degli Abruzzi 24, 10129 Torino, Italy

WILLIAM LIBONI
"Un Passo Insieme" ONLUS Foundation, Valdellatorre, Torino, Italy

U. RAJENDRA ACHARYA
Department of Electronics and Computer Engineering, Ngee Ann Polytechnic, Singapore, 599489.
Department of Biomedical Engineering, SIM University, Singapore

LIM WEI JIE EUGENE
Department of Electronics and Computer Engineering, Ngee Ann Polytechnic, Singapore, 599489.

MARIANNO FRANZINI
…

SERGIO PANDOLFI
…

GIOVANNI RICEVUTI
…

FRANCESCO VAIANO
…

LUIGI VALDENASSI
…

VINCENZO SIMONETTI
"Kaos" ONLUS Foundation, Torino, Italy

Ozone major autohemotherapy is effective in reducing the symptoms of Multiple Sclerosis (MS) patients, but its effects on brain are still not clear. In this work, we have monitored the changes in the cerebrovascular pattern of MS patients and normal subjects during major ozone autohemotherapy by using Near-Infrared Spectroscopy (NIRS) as functional and vascular technique. NIRS signals are analyzed using a combination of time, time-frequency analysis and nonlinear analysis of Intrinsic Mode Function (IMF) signals obtained from Empirical Mode Decomposition (EMD) technique. Our results show that there is an improvement in the cerebrovascular pattern of all subjects

[*] Typeset names in 10 pt Times Roman, uppercase. Use the footnote to indicate the present or permanent address of the author.

indicated by increasing the complexity of the NIRS signals. Hence, we can conclude that the ozone therapy increases the brain metabolism and helps to recover from the lower activity levels which is predominant in MS patients.

Keywords: Ozone autohemotherapy, Near-Infrared Spectroscopy, MANOVA, Multiple Sclerosis, Time – Frequency, Entropy, Empirical Mode Decomposition, Cerebrovascular pattern.

1. Introduction

Ozone therapy has witnessed an increasing set of applications in recent years. Ozone can be administered by major ozone autohemotherapy, which consists in drawning a given amount of venous blood (approximately 240 grams) and then in reinfusing it after it has been added to a mix of oxygen and ozone [1]. Ozone is effective as anti-bacterial, anti-fungine, and anti-viral agent [1], to treat vascular pathologies [2], and generally to improve tissue oxygenation and microcirculation [3,4]. Ozone plays a fundamental role in inflammation: it induces a mild oxidative stress that, in turn, promotes the generation of anti-oxidative species [5]. In fact, animal studies have shown that ozone therapy is effective in protecting organs from reperfusion damages [6,7]. Hence, ozone shows marked vascular and metabolic therapeutic properties.

Multiple sclerosis (MS) is a degenerative neurological pathology characterized by both vascular and metabolic impairments. If the vascular implications of chronic venous insufficiency in MS are still debated [8,9], the increased level of oxidative stress found in MS patients has been clearly demonstrated [10]. Therefore, ozone therapy has a rationale of application as an adjuvant treatment for MS patients.

The quantification of vascular and metabolic cerebral effects of ozone therapy on patients is not a trivial task. In fact, cerebral autoregulation maintains a constant the level of oxygen which is supplied to the brain, independently with possible changes in the systemic oxygen saturation. Therefore, complex methods and techniques are needed to investigate the cerebrovascular and metabolic effects of ozone therapy. In our previous study, we analysed the long-term effects of ozone autohemotherapy in MS patients and controls by using transcranial Doppler sonography and Near-Infrared Spectroscopy (NIRS) [11,12]. Near-infrared spectroscopy (NIRS) is a non-invasive technique that can potentially measure in real-time the vascular and metabolic characteristics of the brain tissues. By using infrared light, NIRS can monitor the changes in the concentrations of the oxygenated (O_2Hb) and reduced (HHb) haemoglobin in brain tissues [13], thus providing vascular and flow related information. Some NIRS devices helps to measure the concentration changes of the cytochrome-c-oxidase, whose concentration is related to the level of mitochondrial activity of the neurons [14], thus to brain metabolism. We documented that ozone autohemotherapy increased the level of oxygen in the brain up to 1.5 hours after the reinfusion of the ozonized blood, without any adverse vascular effect. Moreover, we showed that the MS subjects had an increase in the cytochrome-c-oxidase activity and concentration about 40 minutes after the end of the treatment. This result demonstrated the positive metabolic effect of ozone in reducing the level of oxidative stress and promoting brain metabolism.

Despite its potentialities, the reliability of the NIRS measurements can be decreased by confounding factors; (i) the contribution of skin and superficial vasculature to the absorption of infrared light [15], (ii) concentration of the molecule to track and (iii) noisier and less reliable signal. In fact, some recent NIRS devices introduced a spatially resolved technique to lower the effect of the confounding factors [15] and removed the possibility of measuring the concentration of the cytochrome-c-oxydase.

The NIRS signals, however, carry considerable information in the frequency domain as well. Obrig *et al.* showed that cerebral NIRS signals allow the evaluation of the cerebral vasomotor reactivity and autoregulation [16]. In our previous studies, we combined time and frequency analysis of NIRS signals in order to extract physiological information while trying to avoid the possible noise sources [17–19]. Furthermore, cerebral NIRS signals acquired when the subject is not in resting conditions might be nonstationary in nature; hence, ad-hoc time-frequency analysis should be used [19,20]. Given the complex interaction between infrared light and tissues, NIRS signals are nonlinear in nature. Therefore, the time and time-frequency analysis might be insufficient to capture the subtle variations from the signals, whereas nonlinear techniques can provide more accurate information [18,21–23].

In this paper, we performed a linear and nonlinear analysis of cerebral NIRS signals acquired from MS patients and controls during major ozone

autohemotherapy. The principal aim of this work is to assess the effect of the ozone autohemotherapy on the subjects' cerebral pattern even without monitoring the cytochrome-c-oxydase concentration. The secondary aim is to propose a general framework for the processing of NIRS signals that can lessen the effects of confounding factors, by relying on a robust and local structure based such as the empirical mode decomposition (EMD).

2. Materials and Methods

This section describes the essential steps of the ozone autohemotherapy protocol and the corresponding registration windows. The overall therapy lasted about 3 hours per patient, but the signals were acquired only at specific time steps. This section describes the time, time-frequency, and nonlinear analysis methods used.

2.1. Ozone Autohemotherapy

The major ozone autohemotherapy protocol consists of the following steps:

1. drowning of 240 grams of whole blood from the subjects (in our case from the antecubital vein) by using SanO3 bags (Haemopharm, Milan, Italy);
2. mixing of the blood with 240 ml of O_2/O_3, composed by O_2 at 50%, with an O_3 concentration equal to 40 µg/ml (Medical 95 CPS, Multiossigen, Gorle (BG), Italy);
3. slow blood re-infusion in the same vein.

During the ozone therapy, we acquired NIRS cerebral signals from the left and right forefront of the subjects. We used a NIRO200 device (Hamamatsu Photonics K.K., Japan), equipped by two probes, which consisted of a photo-detector and four infrared LED sources (wavelengths equal to 775, 810, 830 and 910 nm). Each probe was placed on the subject's forehead. To avoid the sinuses, we placed the probes 2 cm away from midline and 1 cm above the supraorbital ridge [17]. The subjects were asked to stay supine, keeping eyes closed and breathing normally. The NIRS device measured in real-time the concentration changes of the O_2Hb and HHb for both the hemispheres. Since we did not find any statistically significant difference in the concentration changes of the two hemispheres (paired *Student's t-test*; $p > 0.8$), we averaged the signals of the two hemispheres. Hence, for each subject, we recorded the O_2Hb and HHb concentrations.

We analyzed the acquired signals in 7 different time intervals, lasting 256 s each:

1. baseline recording;
2. blood drawing;
3. middle of reinfusion;
4. end (last 256 s) of reinfusion;
5. 40 minutes after reinfusion;
6. 1 hour after reinfusion;
7. 1.5 hours after the reinfusion.

We chose these analysis windows in order to observe specific event related and long-term changes. For each window and on each patient, we performed time domain analysis of the signals, by computing the average of the signal values in each of the observation windows.

2.2. Time – Frequency analysis

The NIRS signals are characterized by a marked nonstationary nature and hence time-frequency analysis is needed [11,19,20]. We have used the Choi-Williams (CW) distribution, which belongs to the Cohen's class [20,24] of bilinear time-frequency transforms. The mathematical formulation of the CW is the following:

$$D_{CW}(t,f) = \iint_{32}^{12} x\left(t-\frac{\tau}{2}\right)\left(x^{*}\left(t+\frac{\tau}{2}\right)g(\tau,\theta)\right) e^{j2\pi t}e^{-j2\pi f\tau}\,d\theta\,d\tau \quad (1)$$

where, $D_{CW}(t,f)$ is the time-frequency representation; t and f represent time and frequency, respectively; θ and τ the frequency and time lag, respectively; $g(\tau,\theta)$ the kernel of the CW distribution, which can be expressed as:

$$g(\tau,\theta) = e^{3} = \quad (2)$$

The parameter σ in eq. (2) is called kernel selectivity and it can be tuned in order to avoid interference terms. For biological signal, it is shown that a value in the range 0.1 – 1 is suitable [25]. In our study, we chose the value of 0.5. We computed the CW distributions for O_2Hb and HHb signals in every analysis window. Figure 1.A reports the O_2Hb concentration changes during the baseline recording of healthy subject, and Fig. 1.B is its corresponding CW representation with function of time and frequency. From the time-frequency representation, we computed the relative power in the low-frequency band with function of total power of the signals, for each subject and each time window. The low-frequency band

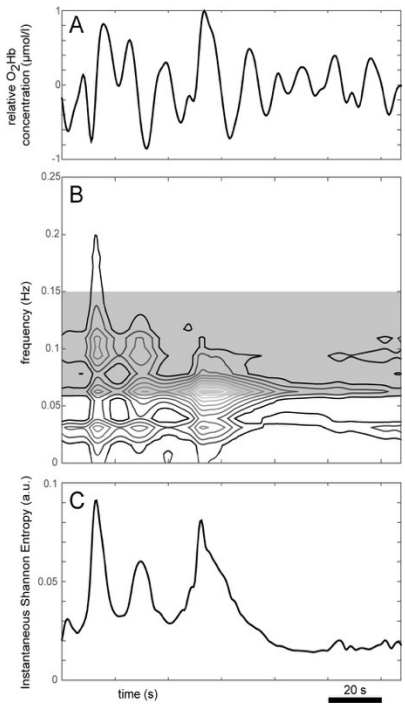

Fig. 1. (A) Time course of the concentration of O_2Hb during baseline. (B) CW transform of the signal. The gray zone represents the LF band. The gray rectangle depicts the LF band. (C) Corresponding instantaneous SE derived from the CW transform.

(LF) spans from about 60 mHz to 150 mHz and it reflects spontaneous oscillations in the cerebral cortex. Such oscillations have a debated physiological meaning; however, they are called as "vasomotor waves" because they reflect the physiological vasomotor reactivity. They are correlated to the firing frequency of the baroceptors, which are the triggers of the regulation of the vascular system [16]. The LF band is depicted by the gray box in Fig. 1.B.

2.3. Instantaneous Shannon Entropy

The Shannon Entropy (SE) is a measure of signal complexity derived in the field of information theory [26]. SE is based on the probability distribution; hence, to make it applicable in signal processing, the power spectral densities must be normalized. However, our signals are nonstationary, so, we defined the SE based on the time-frequency representation $D(t,f)$ of the signals. First of all, we normalized the power of the $D(t,f)$ as follows:

$$d(t,f) = \frac{D(t,f)}{\int_{ED}^{CD}\int D(t,f)\,df\,dt} \qquad (3)$$

in order to make the overall power equal to 1. Then we defined the instantaneous SE as:

$$SE(t) = -\left(\int_{32}^{12} d(t,f)\cdot\ln d(t,f)\right)df \qquad (4)$$

Figure 1.C reports the SE for the signal in fig. 1.A. The time course of the SE was averaged to compute a single value for each signal.

2.4. Empirical Mode Decomposition (EMD)

The empirical mode decomposition is a form of time-frequency representation of the signal that doesn't require linearity. Similar to the Fourier transform, the EMD decomposes the signals into a series of Intrinsic Mode Functions (IMF), which should all have zero *mean* and must be orthogonal[27]. EMD is adaptive and considers the local characteristics of time and scale of the signal. The core of the EMD is the *sifting* procedure, which consists in an iterative algorithm that, at each step, removes from the signal the *mean* of the envelope of the maxima and of the minima of the signal itself. By summarizing, the *sifting* procedure can be described as follows. Let's consider a signal *x(t)*. Let *M(t)* be the spline interpolation of the maxima of the signal, and *m(t)* be the spline interpolation of the minima of the signal. The mean of the two maxima and minima envelopes is computed as $A(t) = [M(t) + m(t)]/2$ and it is subtracted from the signal to generate $h(t) = x(t) - A(t)$. The signal *h(t)* now becomes the new signal and the procedure is repeated until the $h(t)$ is nearly null. At this point, the resulting *h(t)* is named as the first IMF. The extracted IMF is subtracted by the original signal *x(t)* and the procedure is repeated to find the other IMFs. In our work, we considered the first three IMFs of O_2Hb and HHb signals. We have computed two nonlinear metrics: the Sample Entropy (SampEn) and the Hurst Exponent (HE) from the extracted IMFs.

2.5. Sample Entropy (SampEn)

The rationale to compute the SampEn is that this entropy metric is based on the temporal time series instead of relying on the power spectral density[28]. Conceptually, the SampEn is developed to measure the complexity of time series. To quantify this complexity, the time series is used to derive vector sequences of length *m* (called embedding dimension), so that each vector sequence has the form:

$$u(n) = \{h(n), h(n+1), \ldots, h(n+m-1)\} \quad (5)$$

where *h(1), h(2), …, h(N)* are the *N* samples of the time series. The distance between each vector segment and the others is computed by using the Chebyshev distance [29]. Given a distance threshold equal to *r*, each vector sequence is considered and the number of other segments with a distance lower than *r* is computed. This number, divided by the total number of vectors, indicates the probability of locating another vector not beyond the distance *r* from the considered vector $u(n_i)$. Let's call this conditional probability as C^{W}_{UV} The overall conditional probability is given by the sum over the total number of vector sequences:

$$\phi^{W}(r) = (N-m+1) \sum_{i=1}^{N-m+1} C^{W}_{UV}(r) \quad (6)$$

The SampEn is then defined considering also the overall probability found for an embedding dimension equal to *m+1*; hence SampEn is defined as:

$$SampEn(m,N) = -\ln\left[\frac{c^{d}(e)}{c^{dcf}(e)}\right] \quad (7)$$

The basic concept of this metric is that in time series with a high degree of entropy, the vectors (epochs) of length *m* that match point-wise within a tolerance *r* also match at the next point. In our study, we considered a value of *m* equal to 2, and a distance threshold *r* equal to 1.

2.6. Hurst Exponent (HE)

The Hurst exponent (HE) is proposed to measure the presence/absence of long-range in a signal and dependence degree[30]. It quantifies the smoothness of a given time series, because a less complex time series are characterized by a more stable and smooth time course. Hence, the HE is higher for less complex (*i.e.* more correlated) systems and becomes lower when complexity increases.

Given a time series *h(n)* of time length equal to *T*, the mean of the time series is computed and then subtracted by the time series itself. This produces a zero *mean* time series *h'(n)*. The cumulative deviation of *h'(n)* is then computed by summing up all the elements. Let's define *R* as the range of the cumulative deviation of *h'(n)* (*i.e.* the difference between the maximum and the minimum value) and *S* as the standard deviation of *h'(n)*. The HE is then defined as:

$$HE = \frac{hij\,k(m)}{hij\,(n)} \quad (8)$$

For each IMF we calculated the two descriptors related to the complexity of the signals, which are: the Hurst Exponent (HE) and the Sample Entropy (SampEn).

2.7. Patients Demographics

The experiment was conducted after having obtained the approval from the Review Institutional Board of the "Un Passo Insieme ONLUS Foundation" (Valdellatorre, Torino, Italy), of the "KAOS ONLUS Foundation" (Caselle Torinese, Torino, Italy), and of the Italian Society for the Oxygen and Ozone Therapy (SIOOT, Gorle (BG), Italy). The approved informed consent was read and explained to the subjects before the tests and they were required to sign it.

We recruited 10 subjects suffering from Remitting-Relapsing (RR) multiple sclerosis, with a confirmed diagnosis of pathology whose onset was at least five years before. The average age was 39.3±4.0 years, 4 patients were females. In control group, we enrolled 10 volunteers (age: 60.1±4.2 years, 6 females), without any neurological, metabolic, or cardiovascular disease. Heavy smoking and hypertension subjects were excluded. Two MS-RR subjects successfully underwent therapy, but interrupted the recording and did not reach

Table 1. Relative concentrations of O_2Hb and HHb in the analysis windows. The first window is taken as reference.

	Controls		MS-RR group	
	O_2Hb (%)	HHb (%)	O_2Hb (%)	HHb (%)
Window 1	-	-	-	-
Window 2	0.362±2.657	-0.633±0.545	-0.151±1.963	-0.180±0.755
Window 3	0.029±2.394	-0.386±1.436	-0.625±1.463	-0.050±0.750
Window 4	-0.247±2.126	-0.593±1.716	-0.644±2.002	-0.100±0.574
Window 5	1.453±4.549	-0.791±2.223	-1.768±2.474	0.062±0.771
Window 6	1.334±5.004	0.037±1.766	-1.410±2.882	0.045±0.308
Window 7	1.997±4.743	0.201±1.449	0.160±2.489	0.009±0.715

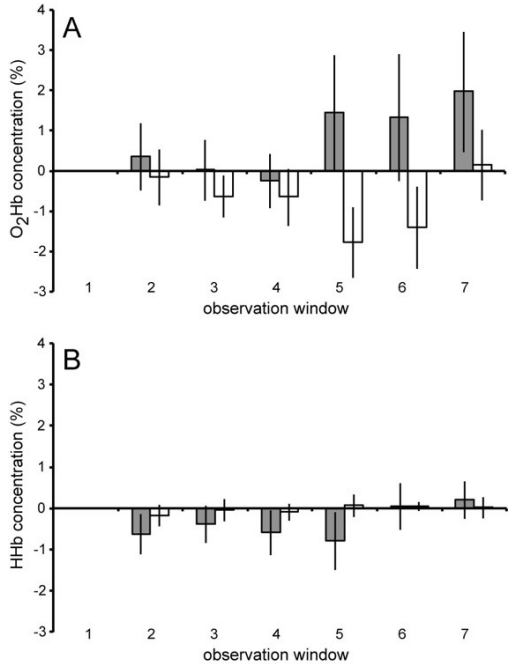

Fig. 2. Time evolution of the average concentration of O2Hb and HHb in the seven analysis windows. All the values are normalized and scaled w.r.t. the first window. Controls are depicted in gray, MS patients in white. The vertical bars superimposed to the hist

the end of the monitoring. These two subjects were excluded from the analysis. Thus, our sample group consists of 8 MS-RR and 10 controls.

2.8. Statistical Analysis

Grouped data are expressed by mean ± SD. The Kolmogorov–Smirnov test is used to test normality of the data, followed by a Student's t-test to check differences in the mean values. For all the tests, the first error species probability is set to 5% (*i.e.* confidence level of 95%). Multivariate analysis of variance (MANOVA) is used to compare the entropy data among the two groups and their change from the beginning to the end of the monitoring. MANOVA represents the subjects in function of the so-called canonical variables, which are linear combination of the original features. The overall number of the original features is 98 for each subject, 14 for each analysis window. The 14 features are the SE of O_2Hb and HHb signals (2 features), and SampEn and HE of the three IMFs from O_2Hb and HHb signals (12 features). Feature reduction is performed by removing the variables that explained a statistically low amount of overall data variability by using the Wilk's lambda [31]. The number of features decreased from 98 to 35 and the MANOVA is performed on these remaining variables. The original features that had the highest number of coefficients in the canonical variables that are considered as most important to assess the changes in the cerebrovascular pattern induced by the ozone therapy and captured by NIRS.

3. Results

In this work, we studied the temporal changes, spectral changes, and the complexity changes of NIRS signals acquired from the brain of MS patients and control subjects during major ozone autohemotherapy. The purpose of this work is to document the vascular and metabolic changes induced by ozone therapy in normal and pathological cerebral tissues.

3.1. Time Changes in Brain Oxygenation

Figure 2 depicts the average concentrations of O_2Hb (fig. 2.A) and HHb (fig. 2.B) signals. The concentrations are normalized and scaled with respect to the first window (baseline), which is thus zero valued. In accordance to previous studies, we found that ozone autohemotherapy increased the level of brain oxygenation both in controls and MS subjects[11,12] (fig. 2.A). There are, however some differences in the two groups. The MS subjects showed a decreasing concentration of O_2Hb, more evident in the 5-th window (40 minutes after the end of blood reinfusion). Then the oxygen concentration raises and reaches positive levels (compared to window 1) at the end of the monitoring, i.e. 1.5 hours after the end of blood reinfusion. Controls, conversely, showed increased O_2Hb concentrations in windows 5 to 7. Figure 2.B demonstrates that the concentration change of HHb, which is not relevant during the therapy and that its variations are statistically equal for MS patients and control subjects. In none of the analysis windows, the concentrations of O_2Hb and HHb are statistically different in MS patients and controls (always $p > 0.2$). The numerical values of concentrations of O_2Hb and HHb are reported in Table 1. None of the concentrations in the different windows are statistically different from zero (*i.e.* from the baseline).

3.2. Frequency Changes in NIRS Signals

Obrig *et al.*[16] shown that, the spontaneous oscillations of NIRS signals can be used to assess the subject's

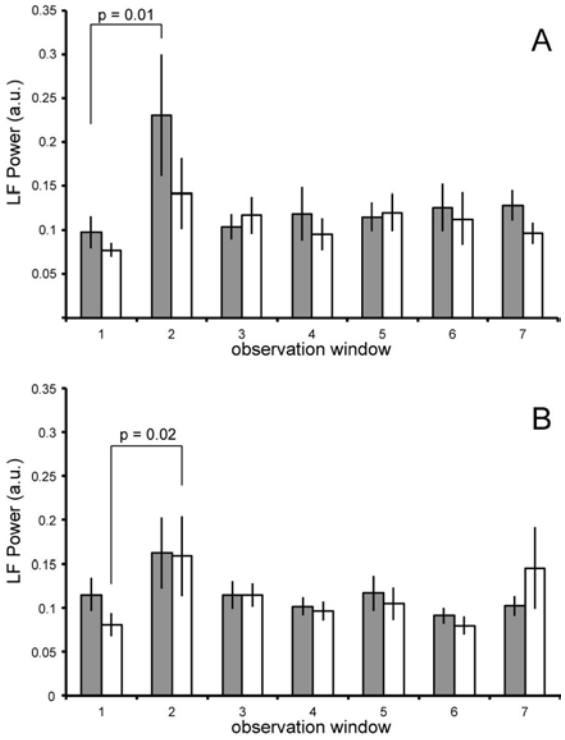

Fig. 3. Changes in the power associated to the LF band compared to the overall signal power. Controls are depicted in gray, MS patients in white. The vertical bars superimposed to the histogram represent the standard error. (A) Power in the LF band for the O_2Hb. (B) Power in the LF band for the HHb.

cerebrovascular reactivity. Our time-frequency analysis showed how the power associated in the LF band, thus in the vasomotor tone, changed during the therapy. Figure 3 represents the changes in the LF power (normalized to the total power of the signal) of control and MS subjects during the therapy. It can be noticed that during blood drawing (window 2), the power in the LF band increased significantly compared to baseline ($p = 0.01$) for the O_2Hb signal of control subjects, and for the HHb signal of MS patients ($p = 0.02$). This effect is due to the vagal response to the needle insertion for blood drawing. In the rest of the therapy, we did not observe significant LF changes in the O_2Hb and HHb signals. Table 2 summarizes the LF relative powers in the seven analysis windows.

3.3. Signals' Entropy and Complexity Changes

The total of 98 complexity descriptors of the signals in the analysis windows are reduced to 35 after the feature selection procedure. These 35 features are considered as descriptive of the complexity of the cerebrovascular pattern of the subjects. The MANOVA is then applied to the set of 35 features per subject in order to evidence differences in the overall cerebrovascular patterns of MS patients versus controls. Figure 4 reports the representation of the subjects in the canonical plane of the first and second variables as computed by MANOVA for three different analysis windows: Fig. 4.A is relative to the baseline (1st window), Fig. 4.B is relative to the end of the blood reinjection (4th window), and fig. 4.C to the end of the monitoring (7th window, approximately 1.5 hours after the end of the reinfusion). In baseline conditions (Fig. 4.A), the MANOVA analysis reveal that it is possible to reject the null-hypothesis that the subjects belonged to the same group ($p = 1.9 \cdot 10^{-4}$). In fact, the MANOVA dimension, which intuitively correspond to the number of variables sufficient to separate groups) is equal to 1. It can be noticed that the MS patients have a positive value of first canonical variable, whereas the controls have a negative one. At the end of the reinjection of the ozonized blood (Fig. 4.B), the dimension of the MANOVA already lowered to zero ($p > 0.5$); thus indicating that it is not possible to reject the hypothesis that the subjects belong to the same group. At the end of the monitoring (Fig. 4.C), the MANOVA dimension is still zero and the subjects belonging to the two different groups are even closer ($p > 0.5$).

Table 2. Relative power in the LF band for the O_2Hb and HHb signals in the analysis windows.

	Controls		MS-RR group	
	O_2Hb (%)	HHb (%)	O_2Hb (%)	HHb (%)
Window 1	0.098±0.059	0.115±0.060	0.077±0.023	0.081±0.037
Window 2	0.231±0.219	0.163±0.128	0.142±0.115	0.159±0.115
Window 3	0.104±0.046	0.115±0.052	0.117±0.059	0.115±0.038
Window 4	0.119±0.096	0.102±0.033	0.096±0.052	0.097±0.031
Window 5	0.116±0.052	0.117±0.064	0.120±0.061	0.105±0.052
Window 6	0.126±0.085	0.091±0.030	0.113±0.083	0.080±0.029
Window 7	0.128±0.053	0.102±0.036	0.096±0.034	0.145±0.131

Table 3. Numerical values of the three most discriminant features in the 1st, 4th, and 7th nalysis windows. The first three rows are relative to controls, the bottom three rows to the MS patients. Overall, the complexity of the IMFs is increasing, with increasing values of sample entropy and decreasing values of the Hurst exponent.

		Window 1	**Window 4**	**Window 7**
Controls	SampEn IMF1 (HHb)	0.370±0.109	0.401±0.132	0.431±0.059
	SampEn IMF3 (O_2Hb)	0.201±0.057	0.244±0.098	0.266±0.091*
	HE IMF1 (HHb)	0.529±0.200	0.406±0.137	0.315±0.132*
MS-RR group	SampEn IMF1 (HHb)	0.387±0.081	0.410±0.109	0.429±0.113
	SampEn IMF3 (O_2Hb)	0.281±0.104	0.287±0.073	0.318±0.076
	HE IMF1 (HHb)	0.518±0.156	0.471±0.148	0.408±0.184

* indicates a statistically significant difference compared to the 1st window

Table 3 reports the the statistical analysis results of three most discriminant features resulting from the Wilk's Lambda analysis. In all the three considered windows, the most significant features are the SampEn of first IMF obtained from HHb signal, the SampEn of the third IMF from O_2Hb signal, and HE of the first IMF from HHb signal. It can be observed that the entropy of the IMF is increasing as effect of ozone therapy, whereas the HE is decreasing. This result is observed on controls and on MS patients as well, although only for controls the increase in the SampEn of IMF3 from

O_2Hb signal and HE of the IMF1 from HHb signal are statistically higher at the end of the monitoring compared to the baseline conditions ($p < 0.001$). The increase in the SampEn and decrease of the HE are both indicators of increasing complexity.

Figure 5 reports the results of three IMFs extracted from HHb signal. The left panel (Fig. 5.A) depicts the signal and its three IMFs during the baseline (1st window). The right panel (Fig. 5.B) depicts the signal and its IMFs at the end of the therapy (7th window). It can be noted that three IMFs actually show a markedly higher complexity at the end of the monitoring (Fig. 5.B). More specifically, the IMF1 during baseline (Fig. 5.A) results in a quasi-periodic signal, clearly dominated by a single frequency. In this condition, it is expected that the entropy is low, due to the repeatability of the signal. Conversely, at the end of the ozone therapy (Fig. 5.B), the same IMF1 is characterized by random bursts of different amplitude and frequency, which make the signal less repeatable and therefore complexity increases.

4. Discussion

There are many literatures discussing the positive effects of the oxygen and ozone therapy on different pathophysiological process[6,7], tissues[22], and organs[1,2,7]. However, there is the need of robust techniques for the in-vivo and real-time monitoring of the ozone effects during a therapy. When ozone is used for therapy on specific tissues or systems, most of the times the validation of the therapeutic effect is done by assessing either the overall improvement of the tissue, or by quantifying some functional markers. As an example, He C. and Ma X. [32] documented an improved distal fallopian tube recanalization and consequent higher number of conceptions in 400 infertile women with tube obstruction treated with ozone. When antibacterial properties are exploited, the validation is usually done by measuring the concentration changes of infective agents or the healing process of tissues. Shah P. *et al.* [4] showed how ozone autohemotherapy is effective in healing the leg of a patient with the post-surgical complications due to *staphylococcus aureus* infection causing a necrotic wound. At a molecular level, Re *et al.* [33] first demonstrated that ozone autohemotherapy helped the synthesis of proteins which collectively favoured cell survival.

When the effects of ozone therapy have to be monitored at a cerebral level, there are limitations on the number of biomarkers that can be non-invasively quantified and on the minimally-invasive techniques that can be used. Cerebral autoregulation masks most of the vascular effects of therapies, since it tend to let the cerebrovascular pattern in a steady-state even in the presence of systemic changes in the concentration of

blood gases or in presence of alterations of the velocity-pressure field. Brain-blood barrier blocks the exchange of many chemical compounds between brain tissue and blood; thus, many markers of inflammation, oxidation, and metabolic functions cannot be directly measured by blood samples. In this study, we adopted the NIRS as a real-time and non-invasive monitoring system to assess the changes induced by the major ozone autohemotherapy in the cerebrovascular pattern. We previously showed that during this kind of therapy, MS patients underwent an increase in the activity level of the cytochrome-c-oxidase of the brain tissues [11,12]. The study is based on the spectral analysis of the NIRS signals by using a time-frequency approach. However, from a signal processing point of view, time-frequency transforms can only capture changes in the power distribution of the signals. But they cannot capture subtle changes in the signal . Also, as mentioned in the introduction, in most of the commercially available NIRS devices, the measurement of the cytochrome-c-oxidase is not available. Hence, to satisfy our first aim, we conducted an extensive time and frequency analysis, and nonlinear analysis of the NIRS signals.

In accordance to previous studies, the ozone therapy increased the overall level of tissue oxygenation [3,6,11]. The oxygen increase is more evident in controls than in MS patients (fig. 2.A). The latter group of subjects reached an actual increase in the level of oxygen concentration only at the end of the monitoring, about 1.5 hours after the end of the reinfusion of the ozonized blood. This result might be explained by the metabolic boost induced by ozone. It is proved that MS patients are characterized by lower level of mitochondrial activity, possibly due to an oxidative damage to the DNA [10,34]. Since ozone improved the level of mitochondrial activity [11], it may be that the increment in the metabolic function of neurons caused an increase in the level of oxygen consumption. Therefore, just after the end of blood reinjection, the oxygen demand could have increased, thus leading to vascular response to increase the concentration at a later stage (about 1 hour after the end of the reinfusion).

This consideration is supported also by the analysis of the relative power in the LF band of the NIRS signals (fig. 3). It can be noticed that a slight (statistically not significant, $p > 0.05$), increase in the LF relative power in the last three observation windows (compared to the 1st window), more evident in the last window of the HHb

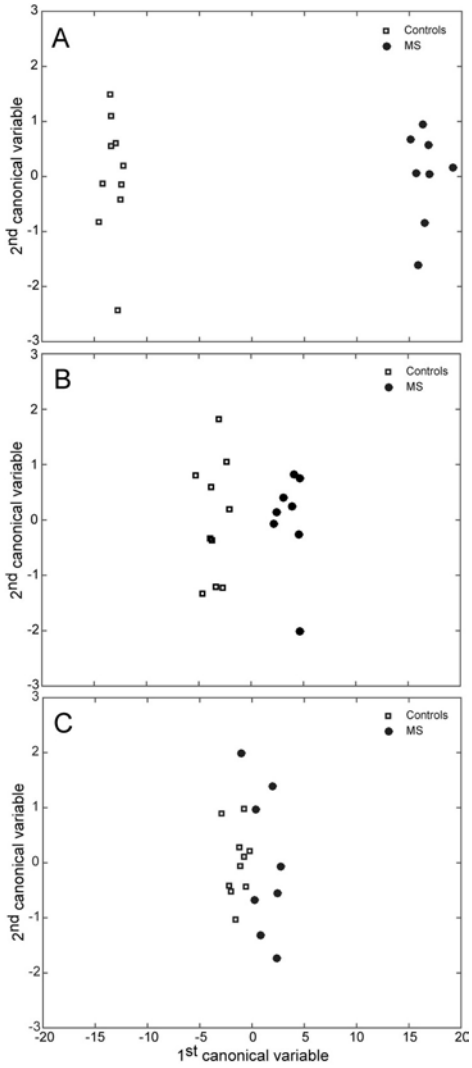

Fig. 4. Representation of the MANOVA analysis for the subjects in three windows during therapy: (A) baseline (1st window); (B) end of the blood reinfusion (4th window); (C) end of monitoring (7th window). Controls are represented by white squares, MS patients by black circles. In (A) the subjects belong to two different groups ($p = 1.9 \cdot 10^{-4}$), whereas in (B) and (C) the hypothesis that the subjects belong to the same group cannot be rejected ($p > 0.5$).

signals analysis (fig. 3.B). Being the LF band a fingerprint of the vasomotor reactivity, this observation supports the hypothesis of increased metabolic demand by the brain cells, which triggers the cerebral autoregulation.

We have coupled a nonlinear analysis of the NIRS signals complexity to the time and time-frequency analysis. We showed that complexity of the cerebrovascular pattern increased during the therapy

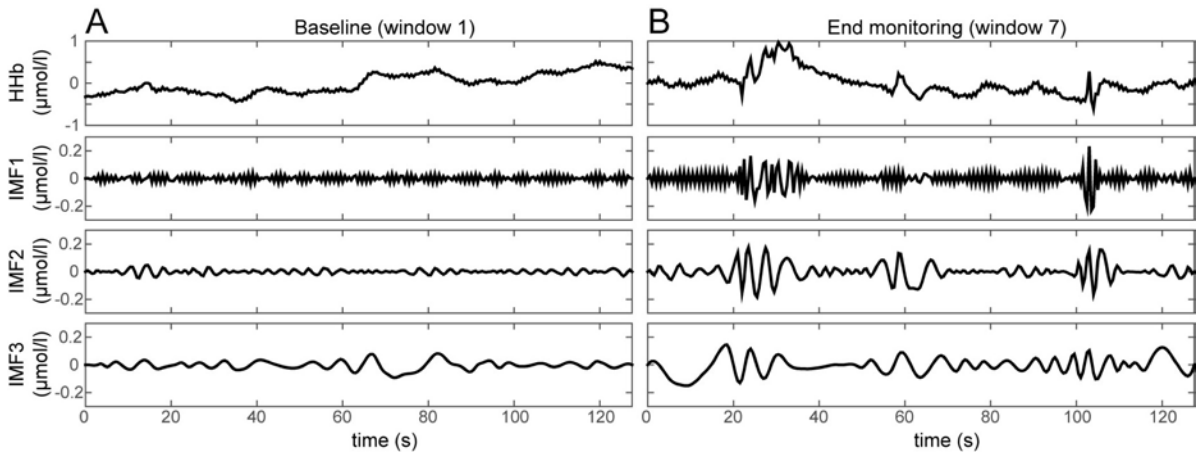

Fig. 5. Results of the empirical mode decomposition applied to the HHb signal acquired in baseline conditions (A) and at the end of the monitoring (B). The upper panels report the HHb time course; then the three IMFs are depicted. It can be observed that in panel (B) the IMFs are characterized by random bursts and changes, which make the signals less predictable and more complex.

(Table 3). Among all the complexity descriptors used, the most significant are the SampEn of the first IMF of the HHb signals and the third IMF of the O_2Hb signals, along with the HE of the first IMF of the HHb signals. These three features explained about 85% of the total variance of the data in the three analysis windows of fig. 4. The increasing values of the SampEn and the decreasing value of the HE reveal an overall increasing complexity of the NIRS signals, both in controls and MS patients. The first IMF obtained from EMD characterizes higher frequencies (fig. 5), whereas the third IMF lower frequencies. Interestingly, the most important feature for the MANOVA analysis is the SampEn of the first IMF of the HHb, which reveals a higher complexity indicating the rapid changes of the signal. Conversely, for the O_2Hb signal, we found that the increase in the complexity was found in the third IMF. The third IMF is characterized by lower frequencies and higher amplitude compared the the first one. This indicates higher complexity in the slower changes of the O_2Hb concentration. This result is in accordance to the time changes reported by fig. 2: the HHb signal did not show major changes during the therapy, while the O_2Hb concentration changed considerably in both two groups. Therefore, the complexity and entropy-based analysis can capture subtle and more accurate differences in the overall cerebrovascular pattern, which are difficult to observe by time and/or time-frequency analysis alone.

It is well known that the complexity of biosignals is linked to the state and properties of the underlying physiological system. In several studies, it is shown how the entropy of the EEG signal can be used to classify the sleep stages[35], and identify[36] and predict[37] epileptic seizures. It is also shown that diabetes mellitus decreased the complexity of the EMG signals[38] of the subjects, and that physical activity helped to restore more complex muscular pattern in diabetic subjects[22]. Complexity of biosignals is usually connected to the unpredictability of the control mechanisms. In this case, since we are monitoring brain vascular and metabolic conditions, an increased complexity could be the effect of an increased level of control by means of cerebral autoregulation. Since the level of cerebral autoregulation is linked to the functional state of neurons, it can be hypothesized that, after a major ozone autohemotherapy, there is a boost in the metabolic and functional response of MS patients which brings the overall cerebrovascular pattern close to that of controls (fig. 4). The complexity of the NIRS signals increases in control subjects. Hence, we can conclude that the ozone autohemotherapy is beneficial to improve the overall cerebrovascular pattern of subjects. Our study shows that changes in the cerebrovascular pattern cannot be properly observed by relying only on time and/or time-frequency analysis. Major changes in oxygen or carbon dioxide concentrations in the brain tissues are clearly linked to blood ozonisation and reinfusion. But they cannot explain which are the positive effects of the therapy at a functional and molecular level. Therefore, more complex frameworks for data analysis are required. In this work, we have shown that, EMD is an efficient tool for the analysis of the cerebral NIRS signals.

The limitations of this study are the number of enrolled subjects is limited. However, being the protocol focused

on the assessment of long-term effects of ozone therapy, it is difficult to find MS patients that can hold the NIRS monitoring for about three hours. NIRS requires continuous monitoring. It is not possible to interrupt the monitoring, detach the probes, and then apply them once again. This will cause a change in the optical coupling that introducing random variability in the signals. In our previous experience we noted that about 50% of the MS subjects could not complete the monitoring due to pain, physiological needs, or excessive stress. Another limitation is that the NIRS equipment we used did not measure the concentration changes of the cytochrome-c-oxidase. To the best of our knowledge, the only reliable biomarker of brain metabolism which can be non-invasively monitored is by NIRS signals. Nevertheless, we believe that our results documented an improvement in the cerebral pattern of the subjects, which also correlated with the subjective sensation of patients and clinical observations. Finally, the two groups are not exactly age-matched. We compared the cerebrovascular pattern of MS patients to a group of controls that was older. As age progresses, the cerebrovascular autoregulation, and therefore the cerebrovascular pattern, worsens even in healthy and asymptomatic subjects. Hence, further studies comparing age-matched groups could be useful to better analyse the cerebrovascular recovery caused by ozone therapy on MS sufferers.

5. Conclusions

In this study, we have analysed the changes in the cerebrovascular pattern of MS patients and normal subjects after a major ozone autohemotherapy. We have observed an increase in the complexity of the cerebrovascular pattern caused due to an increase in the metabolism. The changes in brain metabolism and oxygenation are monitored by a NIRS system. We have shown that time analysis of the NIRS signals is not able to explain the complex effects of ozone therapy. Hence, we have proposed non-linear and complexity features to assess the functional cerebrovascular changes using NIRS signals.

6. Acknowledgements

Part of the study was founded by the Italian Society for Oxygen/Ozone Therapy (SIOOT).

7. References

1. Zaky, S. *et al.* Preliminary results of ozone therapy as a possible treatment for patients with chronic hepatitis C. *J. Altern. Complement. Med.* **17,** 259–63 (2011).
2. Bocci, V., Zanardi, I. & Travagli, V. Ozone: a new therapeutic agent in vascular diseases. *Am. J. Cardiovasc. Drugs* **11,** 73–82 (2011).
3. Clavo, B. *et al.* Ozone Therapy for Tumor Oxygenation: a Pilot Study. *Evidence-based Complement. Altern. Med.* **1,** 93–98 (2004).
4. Shah, P., Shyam, A. K. & Shah, S. Adjuvant combined ozone therapy for extensive wound over tibia. *Indian J. Orthop.* **45,** 376–379 (2011).
5. Sagai, M. & Bocci, V. Mechanisms of Action Involved in Ozone Therapy: Is healing induced via a mild oxidative stress? *Medical Gas Research* **1,** 29 (2011).
6. Di Filippo, C. *et al.* Acute oxygen-ozone administration to rats protects the heart from ischemia reperfusion infarct. *Inflamm. Res.* **57,** 445–449 (2008).
7. Chen, H. *et al.* Ozone oxidative preconditioning inhibits inflammation and apoptosis in a rat model of renal ischemia/reperfusion injury. *Eur. J. Pharmacol.* **581,** 306–14 (2008).
8. Morovic, S. & Zamboni, P. CCSVI is associated with multiple sclerosis. *Neurological Research* **34,** 770–779 (2012).
9. Dake, M. D. Chronic Cerebrospinal Venous Insufficiency and Multiple Sclerosis: History and Background. *Tech. Vasc. Interv. Radiol.* **15,** 94–100 (2012).
10. Lu, F. *et al.* Oxidative damage to mitochondrial DNA and activity of mitochondrial enzymes in chronic active lesions of multiple sclerosis. *J. Neurol. Sci.* **177,** 95–103 (2000).
11. Molinari, F. *et al.* Ozone autohemotherapy induces long-term cerebral metabolic changes in multiple sclerosis patients. *Int. J. Immunopathol. Pharmacol.* **27,** 379–89
12. Lintas, G., Molinari, F., Simonetti, V., Franzini, M. & Liboni, W. Time and time-frequency analysis of near-infrared signals for the assessment of ozone autohemotherapy long-term effects in multiple sclerosis. *Conf. Proc. ... Annu. Int. Conf. IEEE Eng. Med. Biol. Soc. IEEE Eng. Med. Biol. Soc. Annu. Conf.* **2013,** 6171–4 (2013).
13. Elwell, C. E. *et al.* Quantification of adult cerebral hemodynamics by near-infrared spectroscopy. *J. Appl. Physiol.* **77,** 2753–2760 (1994).
14. Arnold, S. The power of life-Cytochrome c oxidase takes center stage in metabolic control, cell signalling and survival. *Mitochondrion* **12,** 46–56 (2012).
15. Canova, D., Roatta, S., Bosone, D. & Micieli, G. Inconsistent detection of changes in cerebral blood volume by near infrared spectroscopy in standard clinical tests. *J. Appl. Physiol.* **110,** 1646–55 (2011).
16. Obrig, H. *et al.* Spontaneous Low Frequency Oscillations of Cerebral Hemodynamics and Metabolism in Human Adults. *Neuroimage* **12,** 623–639 (2000).
17. Molinari, F., Liboni, W., Grippi, G. & Negri, E. Relationship between oxygen supply and cerebral blood flow assessed by transcranial Doppler and near-infrared spectroscopy in healthy subjects during breath-holding. *J. Neuroeng. Rehabil.* **3,** 16 (2006).
18. Molinari, F. *et al.* Empirical mode decomposition analysis of near-infrared spectroscopy muscular signals to assess the effect of physical activity in type 2 diabetic patients.

Comput. Biol. Med. **59,** 1–9 (2015).
19. Liboni, W. *et al.* Why do we need NIRS in migraine? *Neurol. Sci.* **28 Suppl 2,** S222–4 (2007).
20. Molinari, F. *et al.* Time-Frequency Characterization of Cerebral Hemodynamics of Migraine Sufferers as Assessed by NIRS Signals. *EURASIP J. Adv. Signal Process.* **2010,** 459213 (2010).
21. Acharya, U. R. *et al.* Automated diagnosis of epileptic EEG using entropies. *Biomed. Signal Process. Control* **7,** 401–408 (2012).
22. Molinari, F. *et al.* Entropy analysis of muscular near-infrared spectroscopy (NIRS) signals during exercise programme of type 2 diabetic patients: quantitative assessment of muscle metabolic pattern. *Comput. Methods Programs Biomed.* **112,** 518–28 (2013).
23. Faust, O., Acharya, U. R., Molinari, F., Chattopadhyay, S. & Tamura, T. Linear and non-linear analysis of cardiac health in diabetic subjects. *Biomed. Signal Process. Control* **7,** 295–302 (2012).
24. Barry, D. T. Fast calculation of the Choi-Williams time-frequency distribution. *IEEE Trans. Signal Process.* **40,** 450–455 (1992).
25. Molinari, F., Knaflitz, M., Bonato, P. & Actis, M. V. Electrical manifestations of muscle fatigue during concentric and eccentric isokinetic knee flexion-extension movements. *IEEE Trans. Biomed. Eng.* **53,** 1309–1316 (2006).
26. KUMAR, U., Kumar, V. & Kapur, J. N. Normalized Measures of Entropy. *Int. J. Gen. Syst.* **12,** 55–69 (1986).
27. N. E. Huang *et al.* The empirical mode decomposition and the Hilbert spectrum for nonlinear and non-stationary time series analysis. *Proc. R. Soc. London. Ser. A Math. Phys. Eng. Sci.* **454,** 903–995 (1998).
28. Richman, J. S. & Moorman, J. R. Physiological time-series analysis using approximate entropy and sample entropy. *Am. J. Physiol. Heart Circ. Physiol.* **278,** H2039–H2049 (2000).
29. Shieh, M. Z. & Tsai, S. C. Decoding frequency permutation arrays under Chebyshev distance. *IEEE Trans. Inf. Theory* **56,** 5730–5737 (2010).
30. Hurst, H. E. Long-term storage capacity of reservoirs. *Trans. Amer. Soc. Civ. Eng.* **116,** 770–808 (1951).
31. el Ouardighi, A., el Akadi, A. & Aboutajdine, D. Feature Selection on Supervised Classification Using Wilks Lambda Statistic. in *2007 International Symposium on Computational Intelligence and Intelligent Informatics* 51–55 (IEEE, 2007). doi:10.1109/ISCIII.2007.367361
32. He, C. & Ma, X. Distal fallopian tube recanalization using ozone treatment: a clinical study in two hundred tubal obstruction Chinese patients. *Int. J. Clin. Exp. Med.* **8,** 2958–61 (2015).
33. Re, L. *et al.* Is ozone pre-conditioning effect linked to Nrf2/EpRE activation pathway in vivo? A preliminary result. *Eur. J. Pharmacol.* **742,** 158–62 (2014).
34. Broadwater, L. *et al.* Analysis of the mitochondrial proteome in multiple sclerosis cortex. *Biochim. Biophys. Acta - Mol. Basis Dis.* **1812,** 630–641 (2011).
35. Acharya, U. R., Chua, E. C.-P., Chua, K. C., Min, L. C. & Tamura, T. Analysis and automatic identification of sleep stages using higher order spectra. *Int. J. Neural Syst.* **20,** 509–21 (2010).
36. ACHARYA, U. R., SREE, S. V., ANG, P. C. A., YANTI, R. & SURI, J. S. APPLICATION OF NON-LINEAR AND WAVELET BASED FEATURES FOR THE AUTOMATED IDENTIFICATION OF EPILEPTIC EEG SIGNALS. *Int. J. Neural Syst.* (2012). at <http://www.worldscientific.com/doi/abs/10.1142/S0129065712500025>
37. Martis, R. J. *et al.* Application of intrinsic time-scale decomposition (ITD) to EEG signals for automated seizure prediction. *Int. J. Neural Syst.* **23,** 1350023 (2013).
38. Watanabe, K., Miyamoto, T., Tanaka, Y., Fukuda, K. & Moritani, T. Type 2 diabetes mellitus patients manifest characteristic spatial EMG potential distribution pattern during sustained isometric contraction. *Diabetes Res. Clin. Pract.* **97,** 468–73 (2012).